ACS Macro Letters

Letter

pubs.acs.org/macroletters

Structural Evolution of Polylactide Molecular Bottlebrushes: Kinetics Study by Size Exclusion Chromatography, Small Angle Neutron Scattering, and Simulations

Suk-kyun Ahn,*[,†] Jan-Michael Y. Carrillo,*[,‡] Youngkyu Han,[§] Tae-Hwan Kim,[∥] David Uhrig,[†] Deanna L. Pickel,[†] Kunlun Hong,[†] S. Michael Kilbey, II,[⊥] Bobby G. Sumpter,[†,#] Gregory S. Smith,[§] and Changwoo Do*[,§]

[†]Center for Nanophase Materials Sciences, [‡]National Center for Computational Sciences, [§]Biology and Soft Matter Division, Neutron Sciences Directorate, and [#]Computer Science and Mathematics Division, Oak Ridge National Laboratory, Oak Ridge, Tennessee 37831, United States

[⊥]Departments of Chemistry and Chemical and Biomolecular Engineering, University of Tennessee, Knoxville, Tennessee 37996, United States

[∥]Neutron Science Division, Department of Reactor Utilization and Development, Korea Atomic Energy Research Institute, 1045 Daedeok-daero, Yuseong-gu, Daejeon, Republic of Korea

Supporting Information

ABSTRACT: Structural evolution from poly(lactide) (PLA) macromonomer to resultant PLA molecular bottlebrush during ring opening metathesis polymerization (ROMP) was investigated for the first time by combining size exclusion chromatography (SEC), small-angle neutron scattering (SANS), and coarse-grained molecular dynamics (CG-MD) simulations. Multiple aliquots were collected at various reaction times during ROMP and subsequently analyzed by SEC and SANS. These complementary techniques enable the understanding of systematic changes in conversion, molecular weight and dispersity as well as structural details of PLA molecular bottlebrushes. CG-MD simulation not only predicts the experimental observations, but it also provides further insight into the analysis and interpretation of data obtained in SEC and SANS experiments. We find that PLA molecular bottlebrushes undergo three conformational transitions with increasing conversion (i.e., increasing the backbone length): (1) from an elongated to a globular shape due to longer side chain at low conversion, (2) from a globular to an elongated shape at intermediate conversion caused by excluded volume of PLA side chain, and (3) the saturation of contour length at high conversion due to chain transfer reactions.

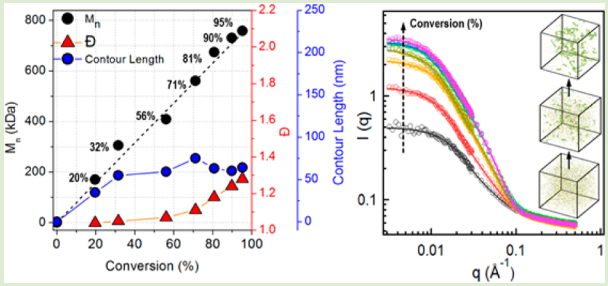

Monitoring polymerization kinetics provides valuable details of reaction characteristics,[1] including rate constants, reactivity ratios of monomers as well as reactivities of catalyst/initiators. Understanding the polymerization kinetics, therefore, plays a central role in identifying the underlying polymerization mechanism (e.g., step- vs chain-growth).[2] Kinetic studies of numerous polymerizations have been performed using various spectroscopic methods, such as Fourier-transform infrared (FT-IR),[3] nuclear magnetic resonance (NMR),[4] UV−vis,[5] and fluoresence spectroscopy,[6] as well as size exclusion chromatography (SEC).[2,7] Spectroscopic methods provide insights into changes in chemical structures and functional groups, while SEC provides information about changes in molecular weight, dispersity, and viscosity. However, these techniques offer only limited insight into changes in polymer structure and chain conformation during polymerizations. In this regard, scattering methods have distinct advantages for elucidating how the shape and size of polymers evolve as polymerization proceeds.[8]

Here we report a convenient and robust methodology for investigating polymerization kinetics of molecular bottlebrushes using complementary SEC and neutron scattering techniques as well as coarse-grained molecular dynamics (CG-MD) simulations. Molecular bottlebrushes are a special class of comb-shaped macromolecules in which relatively short polymeric side chains are densely grafted along the polymer backbone.[9] Unlike linear polymers, these nonlinear macromolecules can adopt a persistent, cylindrical conformation in solution that is largely affected by the molecular and environmental parameters, including the lengths of the backbone and side chains, grafting density of side chains and solvent quality, for example.[10] Previous studies of polymerization kinetics of molecular bottlebrushes have mostly involved only SEC,[7,11] and as a

Received: June 10, 2014
Accepted: August 13, 2014
Published: August 18, 2014

result, to the best of our knowledge, the structural evolution of this class of macromolecules during polymerization has not been reported. This reticence may be due in part to challenges in properly analyzing scattering results because growing bottlebrushes and precursor macromolecules coexist in the polymerization mixture when bottlebrushes are made by the "grafting-through" (or macromonomer) strategy.[7,12]

By using appropriate models to analyze small-angle neutron scattering (SANS), we have efficiently decoupled the scattering contributions of molecular bottlebrushes and precursor macromolecules. Furthermore, our experimental results are compared to those obtained by CG-MD simulations, which not only qualitatively predict our experimental results but also provide additional insight into the polymerization kinetics and structural evolution of molecular bottlebrushes.

As a model system, poly(lactide) (PLA) molecular bottlebrushes were synthesized by ring-opening metathesis polymerization (ROMP) of a norbornenyl PLA macromonomer, as shown in Figure 1a. These PLA molecular

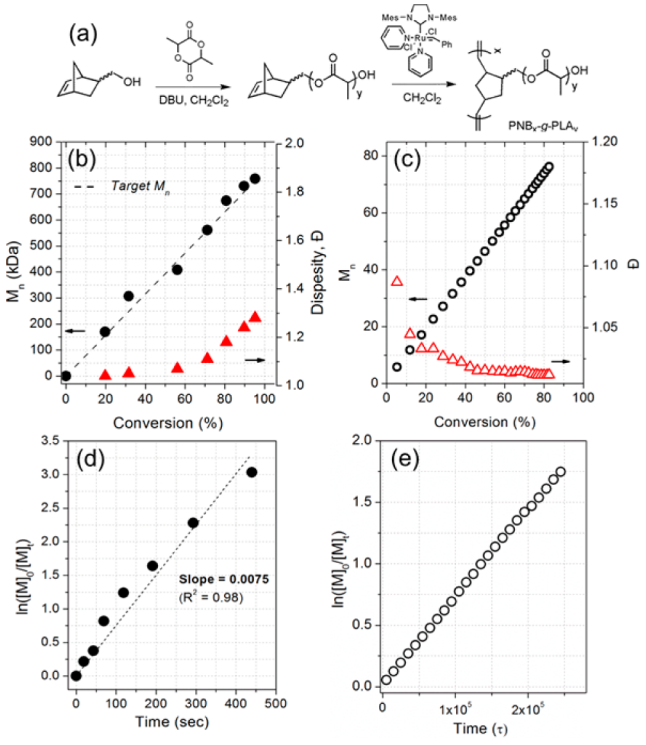

Figure 1. (a) Reaction scheme for syntheses of PLA macromonomer and PLA molecular bottlebrush. (b, c) Changes in molecular weight, M_n, and dispersity, $Đ$, as a function of conversion based on data from experiment (b) and from simulation (c). (d, e) Dependence of $\ln([M]_0/[M]_t)$ on polymerization time from (d) experiment and from (e) simulation.

bottlebrushes are identified as PNB$_x$-*g*-PLA$_y$, where x and y represent degree-of-polymerization of the poly(norbornene) (PNB) backbone (DP_{BB}) and the PLA side chains (DP_{SC}), respectively. The grafting through strategy ensures that each PNB backbone repeat unit has a grafted PLA side chain. Detailed synthetic protocols for syntheses of the norbornenyl PLA macromonomer and PLA molecular bottlebrushes, as well as their characterization can be found in the Supporting Information (Figures S1 and S2 and Table S1). In the current study of polymerization kinetics, we use a constant molecular weight (or the length) of the PLA side chain ($M_{n,NMR}$ = 1570 g/mol or 20 repeat units of lactide, and $Đ$ = 1.27) and vary only the length of the PNB backbone. As a result, conformational changes of PLA molecular bottlebrushes are systematically examined as a function of backbone length.

Polymerization kinetics from PLA macromonomer ($[M]$ = 31.7 mM) to PLA molecular bottlebrush was first investigated using SEC: seven aliquots were collected at various intervals during ROMP and subsequently analyzed by SEC. We observe that the ROMP reaction is very fast, with DP_{BB} reaching 108 within 19 s (PNB$_{108}$-*g*-PLA$_{20}$). Therefore, due to the challenge of collecting multiple aliquots having DP_{BB} less than 108, PLA molecular bottlebrushes (PNB$_{16}$-*g*-PLA$_{20}$, PNB$_{39}$-*g*-PLA$_{20}$, and PNB$_{73}$-*g*-PLA$_{20}$) having low molecular weight were synthesized separately (i.e., nonkinetic samples). This allows a wider range of PLA bottlebrush molecular weights to be examined. We also simulated the living polymerization of the macromonomers by CG-MD simulation, where the backbone and side chain monomers are represented as Lennard-Jones beads of size, σ with finitely extensible nonlinear elastic (FENE) bonds to define the molecular bottlebrush architecture. The details of the simulation are presented in the Supporting Information.

Both SEC and CG-MD simulation results show a linear relationship between molecular weight of PLA molecular bottlebrushes and conversion (Figure 1b,c), and growth of the bottlebrush follows first-order kinetics (Figure 1d,e). The results also suggest that the polymerization is well-controlled. However, a marked difference in dispersity ($Đ$) is observed in the experimental results, where $Đ$ at high conversions increases in contrast with the simulation results. This discrepancy may be due to inter- and intrachain transfer reactions occurring during ROMP,[13] which are not considered in the simulations.

To understand the structural evolution of PLA molecular bottlebrushes, the aliquots collected during ROMP were investigated by SANS. The results shown in Figure 2a show that the scattered intensity at low values of wavevector transfer, q, gradually increases as conversion increases. This trend is expected because as conversion increases, the scattering becomes dominated by the larger PLA molecular bottlebrushes, rather than by the macromonomers. The slope at low q is related to polymer conformation, and the fact that this slope increases with conversion suggests that the shape elongates with conversion. Qualtitavely similar changes are seen in the scattering curves determined from simulations, which are depicted in Figure 2b.

The SANS data were fit using the flexible cylinder model in which internal density fluctuation[10a,14] and the existence of macromonomers were considered. First, in the case of PLA molecular bottlebrushes, scattering contributions from side chains and their fuzzy density profiles of the cross section predominate at high q. Thus, the scattering term of the side chains, which are described by self-avoiding random walks with excluded volume interactions on smaller length scales than the correlation length, is included. Second, because each aliquot contains both macromonomers and PLA molecular bottlebrushes, scattering contributions from both are considered by simply adding a flexible cylinder model for the macromonomers to the modified flexible cylinder model with internal density fluctuation for the PLA bottlebrushes, based on the assumption of dilute concentrations for both. As the percent conversion obtained by SEC analysis is used to determine the relative amount of macromonomers and PLA molecular bottlebrushes in each aliquot collected during ROMP, the relative volume

dx.doi.org/10.1021/mz5003454 | ACS Macro Lett. 2014, 3, 862−866

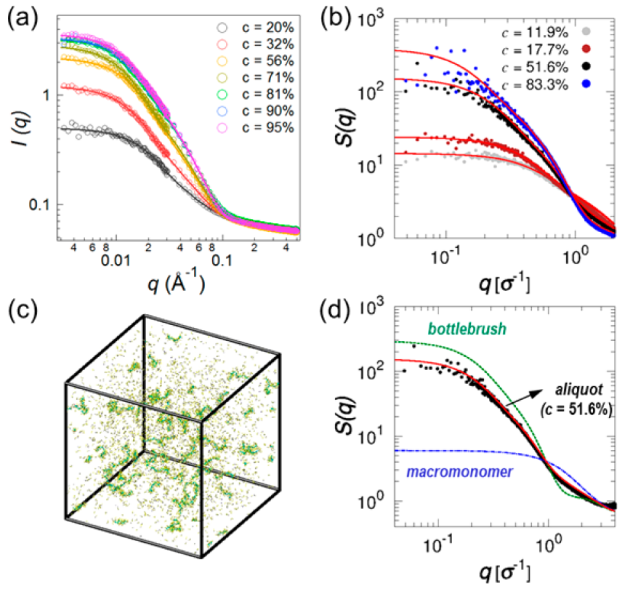

Figure 2. (a) SANS curves of PLA molecular bottlebrushes in THF-d_8 (c = 10 mg/mL) collected at different times during ROMP. Data were fit using the sum of two flexible cylinder models. (b–d) CG-MD simulation results: (b) points are the scattering function, $S(q)$ of the particles in the simulation box, and red lines are calculated form factor, $P(q)$ of the macromonomer and bottlebrush mixture, which are the weighted number-average form factor, $P(q)$ of pure bottlebrushes and pure macromonomers at various conversions; (c) snapshot of the simulation box at 51.6% conversion; (d) form factor, $P(q)$ of mixture, pure bottlebrush, pure macromonomer, and $S(q)$ of the particles in the simulation box at 51.6% conversion.

fraction of macromonomers and PLA bottlebrushes is fixed during the fitting process. To reduce the number of fitting parameters, contour length, Kuhn length, and radius of macromonomers were obtained from a separate analysis of scattering data acquired from the macromonomer solution, and these parameters were assumed to be constant. Further details are provided in the Supporting Information. By simultaneously fitting all of the scattering curves in Figure 2a, the contour length, Kuhn length, and radius of a flexible cylinder representing PLA bottlebrushes are obtained. Also, because the conversion of the independently prepared PLA bottlebrushes (PNB_{16}-g-PLA_{20}, PNB_{39}-g-PLA_{20}, and PNB_{73}-g-PLA_{20}) were nominally 100%, their scattering curves were fit separately without considering macromonomers. However, for these lower DP_{BB} bottlebrushes, an ellipsoid model was also considered, which may be more appropriate than the flexible cylinder model for smaller bottlebrushes.[10b,15] Fitted parameters for the flexible cylinder and the ellipsoid models are summarized in Table 1.

A similar procedure was used for the simulation results, with Figure 2c showing a snapshot of the simulation box having both macromonomers and bottlebrushes. The scattering of each component in the simulation box, which can be captured easily by CG-MD simulation, is shown in Figure 2d. Indeed, the scattering function, $S(q)$ of the particles in the simulation box can be exactly fit by the weighted number-average of the form factor, $P(q)$, of both macromonomers and bottlebrushes. The details for calculating $S(q)$ and $P(q)$ in the simulations are also described in the Supporting Information.

Figure 3a presents the variation in the contour length (L) and twice the semimajor axis ($2r_b$) extracted from flexible

Table 1. Fitted Parameters from Flexible Cylinder and Ellipsoid Models

	flexible cylinder			ellipsoid		
polymer	L[a] (Å)	$R_{cs,g}$[b] (Å)	$R_{g,calcd}$[c] (Å)	r_a[d] (Å)	r_b[e] (Å)	$R_{g,calcd}$[f] (Å)
PNB_{16}-g-PLA_{20}	19.7	22.6		24.0	44.8	30.3
PNB_{39}-g-PLA_{20}	84.8	22.7		27.9	52.8	35.6
PNB_{73}-g-PLA_{20}	159.8	22.8	46.0	27.5	68.7	45.2
PNB_{108}-g-PLA_{20}	360.3	22.4	73.3			
PNB_{195}-g-PLA_{20}	522.4	22.4	99.2			
PNB_{260}-g-PLA_{20}	536.1	22.4	100.9			
PNB_{357}-g-PLA_{20}	617.2	22.4	116.3			
PNB_{429}-g-PLA_{20}	509.9	22.4	105.5			
PNB_{466}-g-PLA_{20}	507.9	22.4	102.1			
PNB_{483}-g-PLA_{20}	546.1	22.4	106.6			

[a]Contour length of a flexible cylinder. [b]Cross section radius of gyration of a flexible cylinder. $R_{cs,g} = (R_b^2/2 + 4\sigma^2)^{1/2}$, where R_b is the core radius of the cylinder and σ is the standard deviation of the Gaussian density profile. [c]Radius of gyration of PLA bottlebrushes is calculated by eq S17. [d]Semiminor axis length. [e]Semimajor axis length. [f]Radius of gyration, calculated based on a prolate ellipsoid.

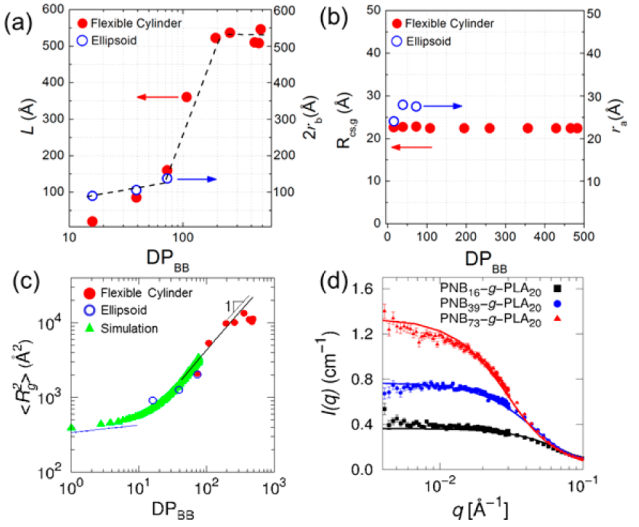

Figure 3. (a) Contour length (L) and twice the semimajor axis ($2r_b$) of PLA molecular bottlebrushes at various DP_{BB}: dashed line is to guide the eye. (b) Cross section radius of gyration ($R_{cs,g}$) and semiminor axis (r_a) of PLA molecular bottlebrushes at various DP_{BB}. (c) Mapping of calculated $\langle R_g^2 \rangle$ from fits of SANS data with simulation data using eq S17 shifted by a constant of 300 Å^2. Solid line is the fit from eq S17 for DP_{BB} > 40 and green triangles are $\langle R_g^2 \rangle$ from simulations. The blue line serves to guide the eye and highlights the transition of power law scaling behavior. (d) Scattered intensity of three nonkinetic samples (datum points) with their corresponding intensity (lines) from simulated bottlebrushes of the same DP_{BB}. The matching of the lines and points arises using a conversion factor of backbone bead diameter, 1σ = 5.13 Å.

cylinder and ellipsoid models, respectively, as a function of DP_{BB} in a semilog fashion. Two noticeable conformational transitions are observed: the region where DP_{BB} changes from low to intermediate values and, subsequently, the region where DP_{BB} changes from intermediate to high values. The former conformational transition is associated with the PLA bottlebrushes undergoing a conformational change from globular to elongated in shape; this transition also has been observed for other types of molecular bottlebrushes.[12c,16] At low DP_{BB}, the

dx.doi.org/10.1021/mz5003454 | ACS Macro Lett. 2014, 3, 862–866

PLA side chain is more influential, and the molecular conformation of the small PLA bottlebrushes is close to that of a globular object. However, if the length of backbone is sufficiently long, longer than that of side chain, the extended cylindrical conformation is favored due to strong excluded volume effect of PLA side chains. This conformational transition explains why an apparent sharp increase in contour length is observed.

The latter conformational transition, which results from a saturation of contour length and is observed after 71% conversion (or DP_{BB} = 361), suggests that the average size of molecular bottlebrushes no longer increases. This seemingly unexpected behavior is associated with the dramactic increase in the dispersity for PLA molecular bottlebrushes at higher conversions (Figure 1b). Molecular weight distributions of three largest PLA molecular bottlebrushes show only a slight shift in peak molecular weight (M_p) and a long tail toward longer retention time, implying that there is an increase in the amount of smaller PLA molecular bottlebrushes in these samples caused by chain transfer reactions (Figure S3). As a result of the increasing scattering contribution from smaller PLA molecular bottlebrushes, the steady increment of contour length is limited.

When fitting the values of cross section radius of gyration, σ was assumed to be independent of DP_{BB} because the PLA side chain length has been kept constant throughout the samples. Individually fitted R_b shows very little variation and, therfore, results in $R_{cs,g}$ being nearly constant, as expected (Figure 3b). From atomistic MD simulations, the radius of gyration of the PLA side chains is estimated to be ~10 Å, suggesting quantitative agreement with the $R_{cs,g}$ determined for the molecular bottlebrushes.[10d] It is also interesting to note that the r_a from the ellipsodial model used to fit samples of low DP_{BB} are comparable to $R_{cs,g}$ from flexible cylinder model fits, suggesting that reasonable dimensions were obtained from both fittings.

In Figure 3c we map the calculated mean squared radius of gyration from the SANS experiment with the $\langle R^2_g \rangle$ determined from CG-MD simulations. The mapping utilizes the SANS intensities of three nonkinetic samples (PNB_{16}-*g*-PLA_{20}, PNB_{39}-*g*-PLA_{20}, and PNB_{73}-*g*-PLA_{20}) and their corresponding CG-MD simulation frames having the same value of DP_{BB}. It is possible to use these points for the mapping because, due to complete conversion, the scattering from these samples is dominated by the bottlebrushes, but not by the macromonomers.

Figure 3d illustrates the matching of the calculated scattering intensities from the CG-MD and the nonkinetic samples. The scattered intensities from the CG-MD simulations were scaled to match the experimental SANS data where the scaling in the *x*-axis provided the conversion factor of the coarse-grained bead diameter (σ = 5.13 Å). This conversion factor only pertains to the bead diameter of the bottlebrush backbone, since only DP_{BB} was matched; hence, another step is required to match the bead diameter of the side chains.

The agreement between CG-MD and experiments in Figure 3c is finally realized when the fit using eq S17 for DP_{BB} > 40 (black line), and the simulation data (green triangles) are shifted in the *y*-axis by 300 $Å^2$. The rationale behind shifting by this constant is that it compensates for the size mismatch between the side chain bead in the simulations with that of a real macromonomer. To verify the soundness of the shift factor, we note that at the limiting value of DP_{BB} = 1, which pertains to a single macromonomer, the value of the square root of the shift factor ($\sqrt{300}$ Å = 17.3 Å) is on the order of the R_g of the real macromonomer. In using eq S17, we only considered DP_{BB} values greater than 40 because the Kuhn length CG-MD is more or less constant at this interval and $\langle R^2_g \rangle \sim DP_{BB}$ (see discussion in Supporting Information).

The good aggreement between SANS experiment and CG-MD simulation suggests that simulation can provide clarifying insights of the real-space structure of molecular bottlebrushes that complements the reciprocal space information provided by SANS, which includes the relative shape anisotropy, $\langle \kappa^2 \rangle$ and the largest eigenvalue of the gyration tensor, $\langle \lambda_1^2 \rangle$. Both quantities, shown in Figure 4, illustrate the expected

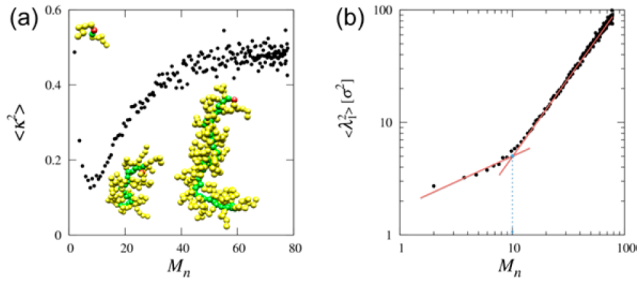

Figure 4. (a) Dependence of $\langle \kappa^2 \rangle$ as a function of M_n. (b) Dependence of the average value of the largest eigenvalue, $\langle \lambda_1^2 \rangle$, as a function of M_n. The images in (a) show sample configurations of the molecular bottlebrushes for N = 2, 17, and 40. The lines in (b) show the change in slope that occurs at $M_n \sim 10$.

conformations: initially there is an elongated macromolecule in which the macromonomer length determines the structure, that transitions to a spherically symmetric structure when side chain and backbone lengths are of the same order. Finally, an elongated structure that behaves like a Kratky−Porod worm-like chain governed by the backbone is realized (see Figures 3c, 4, and S12).

The conformational transitions of PLA molecular bottlebrushes during polymerization elucidated by SANS and CG-MD methods are summarized in Figure 5. The first transition

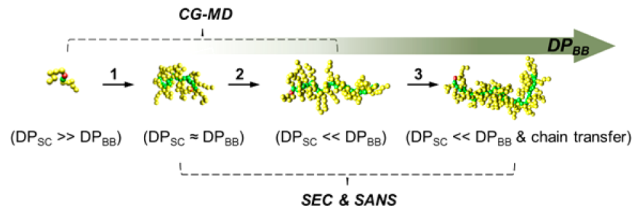

Figure 5. Conformational transitions of PLA molecular bottlebrushes in this study observed by CG-MD (1 and 2) and by SEC and SANS (2 and 3). The transitions are numbered to match the discussion in the text.

(labeled **1** in Figure 5) occurs when the DP of the backbone and side chains are approximately equal. This transition occurs at low DP_{BB}, and is only captured by CG-MD (Figure 4a) because collecting aliquots at low DP_{BB} was practically challenging due to the rapid polymerization. The second transition (labeled **2** in Figure 5), which occurs when the size of the backbone begins to become the dominant length scale, is observed in both SANS and CG-MD (Figures 3a and 4b). The third transition (labeled **3** in Figure 5), which is associated with the saturation of molecular dimension of bottlebrushes at high DP_{BB} (Figure 3a), is observed only by SANS analyses. This

dx.doi.org/10.1021/mz5003454 | *ACS Macro Lett.* 2014, 3, 862−866

transition was not captured by CG-MD because chain transfers were not considered in the simulations.

CG-MD also complements the experimental analysis of SANS data in the fitting procedure. CG-MD steered the fitting toward the assumption that the Kuhn length in the flexible cylinder model is not constant across the range of DP_{BB} accessed in the experiments (Figure S7). This is demonstrated in Figure S13 where CG-MD simulation results show an increase in the persistance length, which is half of the Kuhn length, as a function of DP_{BB}.

In conclusion, polymerization kinetics of PLA molecular bottlebrushes is investigated for the first time using a combination of SEC, SANS, and CG-MD simulation. Using the parameters obtained by SEC, structural details of PLA molecular bottlebrushes are successfully extracted by analyzing SANS data. CG-MD simulation can qualitatively predict polymerization kinetics and provide further insight into structural changes in PLA molecular bottlebrushes. When increasing length of PNB backbone at constant length of PLA side chain, three types of conformational transitions of PLA molecular bottlebrushes are observed: (1) from elongated macromolecules to globular shape of bottlebrushes at low DP_{BB}, (2) from globular to elongated shape of bottlebrushes at intermediate DP_{BB}, and (3) the saturation of the molecular dimension of bottlebrushes at high DP_{BB}. The complementary nature of SEC, SANS, and CG-MD provides a general and robust methodology for understanding structural evolutions of architecturally complex polymers during polymerization with great detail.

■ ASSOCIATED CONTENT

Supporting Information

Details of synthetic protocols, molecular characterizations, scattering models, and CG-MD methods and results are described. This material is available free of charge via the Internet at http://pubs.acs.org.

■ AUTHOR INFORMATION

Corresponding Authors

*E-mail: ahns1@ornl.gov.
*E-mail: carrillojy@ornl.gov.
*E-mail: doc1@ornl.gov.

Notes

The authors declare no competing financial interest.

■ ACKNOWLEDGMENTS

Research at Oak Ridge National Laboratory's Spallation Neutron Source and Center for Nanophase Materials Sciences is sponsored by the Scientific User Facilities Division, Office of Basic Energy Sciences, U.S. Department of Energy. This research used resources of the Leadership Computing Facility at Oak Ridge National Laboratory, which is supported by the Office of Science of the U.S. Department of Energy under Contract No. DE-AC05-00OR22725 with UT-Battelle, LLC. This work was also supported by the HANARO center of Korea Atomic Energy Research Institute and Ministry of Science, ICT and Future Planning (MSIP), Korea government, through its National Nuclear Technology Program (2012M2A2A6004260). S.M.K. acknowledges support from the Sustainable Energy and Education Research Center (SEERC) at Univ. of Tennessee–Knoxville. J.M.C. thanks Prof. A. Dobrynin for his fruitful discussion.

■ REFERENCES

(1) Reed, W. F.; Alb, A. M. *Monitoring Polymerization Reactions: From Fundamentals to Applications*; Wiley: NJ, 2014.

(2) (a) Iovu, M. C.; Sheina, E. E.; Gil, R. R.; McCullough, R. D. *Macromolecules* **2005**, *38*, 8649. (b) Yokoyama, A.; Miyakoshi, R.; Yokozawa, T. *Macromolecules* **2004**, *37*, 1169. (c) Shipp, D. A.; Matyjaszewski, K. *Macromolecules* **1999**, *32*, 2948.

(3) (a) Lizotte, J. R.; Long, T. E. *Macromol. Chem. Phys.* **2004**, *205*, 692. (b) Messman, J. M.; Storey, R. F. *J. Polym. Sci., Part A: Polym. Chem.* **2004**, *42*, 6238. (c) Puskas, J. E.; Long, T. E.; Storey, R. F. *In Situ Spectroscopy of Monomer and Polymer Synthesis*; Springer: New York, 2003.

(4) (a) Cutié, S. S.; Smith, P. B.; Henton, D. E.; Staples, T. L.; Powell, C. *J. Polym. Sci., Part B: Polym. Phys.* **1997**, *35*, 2029. (b) Preusser, C.; Hutchinson, R. A. *Macromol. Symp.* **2013**, *333*, 122.

(5) (a) Husmann, R.; Wertz, S.; Daniliuc, C. G.; Schäfer, S. W.; McArdle, C. B.; Studer, A. *Macromolecules* **2014**, *47*, 993. (b) Lamps, J. P.; Catala, J. M. *Macromolecules* **2009**, *42*, 7282.

(6) Miller, K. E.; Burch, E. L.; Lewis, F. D.; Torkelson, J. M. *J. Polym. Sci., Part B: Polym. Phys.* **1994**, *32*, 2625.

(7) Ahn, S.-k.; Pickel, D. L.; Kochemba, W. M.; Chen, J.; Uhrig, D.; Hinestrosa, J. P.; Carrillo, J.-M.; Shao, M.; Do, C.; Messman, J. M.; Brown, W. M.; Sumpter, B. G.; Kilbey, S. M. *ACS Macro Lett.* **2013**, *2*, 761.

(8) (a) Motokawa, R.; Koizumi, S.; Zhao, Y.; Hashimoto, T. J. *Appl. Crystallogr.* **2007**, *40*, s645. (b) Niu, A.; Stellbrink, J.; Allgaier, J.; Richter, D.; Hartmann, R.; Domski, G. J.; Coates, G. W.; Fetters, L. J. *Macromolecules* **2009**, *42*, 1083. (c) Terashima, T.; Motokawa, R.; Koizumi, S.; Sawamoto, M.; Kamigaito, M.; Ando, T.; Hashimoto, T. *Macromolecules* **2010**, *43*, 8218. (d) Ji, W.; Yan, J.; Chen, E.; Li, Z.; Liang, D. *Macromolecules* **2008**, *41*, 4914. (e) Alb, A. M.; Mignard, E.; Drenski, M. F.; Reed, W. F. *Macromolecules* **2004**, *37*, 2578. (f) Lund, R.; Willner, L.; Richter, D.; Lindner, P.; Narayanan, T. *ACS Macro Lett.* **2013**, *2*, 1082.

(9) (a) Zhang, M.; Müller, A. H. E. *J. Polym. Sci., Part A: Polym. Chem.* **2005**, *43*, 3461. (b) Sheiko, S. S.; Sumerlin, B. S.; Matyjaszewski, K. *Prog. Polym. Sci.* **2008**, *33*, 759. (c) Rzayev, J. *ACS Macro Lett.* **2012**, *1*, 1146. (d) Peng, S.; Bhushan, B. *RSC Adv.* **2012**, *2*, 8557.

(10) (a) Rathgeber, S.; Pakula, T.; Wilk, A.; Matyjaszewski, K.; Beers, K. L. J. *Chem. Phys.* **2005**, *122*, 124904. (b) Cheng, G.; Melnichenko, Y. B.; Wignall, G. D.; Hua, F.; Hong, K.; Mays, J. W. *Macromolecules* **2008**, *41*, 9831. (c) Liu, W.; Liu, Y.; Zeng, G.; Liu, R.; Huang, Y. *Polymer* **2012**, *53*, 1005. (d) Zhang, Z.; Carrillo, J.-M.; Ahn, S.-k.; Wu, B.; Hong, K.; Smith, G. S.; Do, C. *Macromolecules* **2014**, DOI: 10.1021/ma500613c.

(11) (a) Xia, Y.; Kornfield, J. A.; Grubbs, R. H. *Macromolecules* **2009**, *42*, 3761. (b) Neugebauer, D.; Theis, M.; Pakula, T.; Wegner, G.; Matyjaszewski, K. *Macromolecules* **2005**, *39*, 584. (c) Zhang, N.; Luxenhofer, R.; Jordan, R. *Macromol. Chem. Phys.* **2012**, *213*, 973.

(12) (a) Hadjichristidis, N.; Pitsikalis, M.; Iatrou, H.; Pispas, S. *Macromol. Rapid Commun.* **2003**, *24*, 979. (b) Li, X.; ShamsiJazeyi, H.; Pesek, S.; Agrawal, A.; Hammouda, B.; Verduzco, R. *Soft Matter* **2014**, *10*, 2008. (c) Pesek, S. L.; Li, X.; Hammouda, B.; Hong, K.; Verduzco, R. *Macromolecules* **2013**, *46*, 6998.

(13) Bielawski, C. W.; Grubbs, R. H. *Prog. Polym. Sci.* **2007**, *32*, 1.

(14) Bolisetty, S.; Rosenfeldt, S.; Rochette, C.; Harnau, L.; Lindner, P.; Xu, Y.; Müller, A. E.; Ballauff, M. *Colloid Polym. Sci.* **2009**, *287*, 129.

(15) Wataoka, I.; Urakawa, H.; Kajiwara, K.; Schmidt, M.; Wintermantel, M. *Polym. Int.* **1997**, *44*, 365.

(16) Hsu, H.-P.; Paul, W.; Rathgeber, S.; Binder, K. *Macromolecules* **2010**, *43*, 1592.